International Journal of Heat and Mass Transfer 65 (2013) 883–892

Contents lists available at SciVerse ScienceDirect

International Journal of Heat and Mass Transfer

journal homepage: www.elsevier.com/locate/ijhmt

Alternative analytical analysis for improved Loschmidt diffusion cell

Ozgur Cekmer [a], Jacob M. LaManna [a], Matthew M. Mench [a,b,*]

[a] Electrochemical Energy Storage and Conversion Laboratory, Department of Mechanical, Aerospace, and Biomedical Engineering, The University of Tennessee, Knoxville, TN 37996, USA

[b] Emissions and Catalysis Research Group, Oak Ridge National Laboratory, Oak Ridge, TN 37831, USA

ARTICLE INFO

Article history:
Received 12 March 2013
Received in revised form 26 June 2013
Accepted 27 June 2013

Keywords:
Loschmidt cell
Effective diffusion coefficient
Finite volume discretization
Porous media
Mass transport

ABSTRACT

To measure gas phase diffusion coefficients across porous media, an apparatus called a Loschmidt diffusion cell is often utilized. In previous studies with such an apparatus, an infinite-length assumption is used to simplify the analytical solution. Experimentally, cell lengths must be quite long and measurement time is very brief to fulfill this assumption. In this study, Fick's second law is applied, and separation of variables with shifted homogeneity technique is performed for data analysis to enable design of a more compact experimental apparatus with extended measurement times and improved precision. The analytical solution is proved by both the inverse-matrix method and finite-volume discretization. Finally, using the new analytical solution obtained, the effective diffusion coefficient is determined for porous media used in fuel cell applications.

1. Introduction

A Loschmidt diffusion cell is a combination of two gas chambers with a removable barrier between them. This apparatus is used for determination of binary and effective diffusion coefficients of gases flowing through porous media. Initially, each chamber contains different gas concentrations. Due to the concentration difference, when the barrier is removed, gas is exchanged until equilibrium is reached. The concentration change at a point as a function of time can be used to determine the diffusion coefficient. Detailed information about Loschmidt diffusion cells can be found in [1].

There are a limited number of published studies about determination of binary and effective gas diffusion coefficient through porous media in fuel cells using a Loschmidt diffusion cell. In the polymer electrolyte fuel cell (PEFC), several types of porous media exist, including the gas diffusion layer (GDL), micro-porous layer (MPL) and the catalyst layer (CL) (Ref. [2, p. 50]). Diffusion transport is critical in these media, which may also be partially saturated.

Göll and Piesche [3] used a macroscopic approach and presented a new computational model for diffusion in porous media. An isothermal diffusion problem in a Loschmidt tube simulation was used for validation of their new model. Shen et al. [4] used the Loschmidt cell to measure the effective gas diffusion coefficients of a dry O_2–N_2 gas pair in dry fuel cell cathode catalyst layers at 25°C. Astrath et al. [5] investigated the effective gas diffusion coefficients of four different types of stainless steel films with different shaped holes using a Loschmidt diffusion cell. Zamel et al. [6] performed experimental determination of the effective diffusion coefficient of an O_2–N_2 gas mixture through Toray TPGH-120 GDL for fuel cells via a Loschmidt cell. A Loschmidt cell was used for the experimental measurement of effective diffusion coefficient through a GDL MPL composite by Chan et al. [7]. Effective gas diffusion through SGL Sigracet 10-series GDL with 0% and 5% PTFE loading without MPL coating and 25-series GDL with 20% PTFE and MPL coating were analyzed. Zamel et al. [8] developed a correlation for the effective gas diffusion coefficient in carbon paper. An in-house Loschmidt cell with a photothermal-deflection probe was employed to measure the effective diffusion coefficient of a GDL with 70% porosity with a CO_2–O_2 gas mixture by Rohling et al. [9].

In all these studies, the series solution, which is introduced in Refs. [10,11], is used for the diffusion coefficient calculations. In this study, Fick's second law of diffusion is applied to the diffusion problem involving a Loschmidt diffusion cell with a porous layer. The analytical solution is proved by both the inverse-matrix method and finite-volume discretization. Finally, by using the obtained analytical solution, the effective diffusion coefficient is determined for a porous sample.

The previous studies referenced Crank [10] and Carslaw and Jaeger [11] for the derivation of the analytical solution of Fick's second law of diffusion. In this study, Haberman's [12] solution to one-dimensional diffusion problems with non-homogenous

* Corresponding author at: Electrochemical Energy Storage and Conversion Laboratory, Department of Mechanical, Aerospace, and Biomedical Engineering, The University of Tennessee, Knoxville, TN 37996, USA. Tel.: +1 865 974 6751; fax: +1 865 974 5274.

E-mail address: mmench@utk.edu (M.M. Mench).

0017-9310/$ - see front matter © 2013 Elsevier Ltd. All rights reserved.
http://dx.doi.org/10.1016/j.ijheatmasstransfer.2013.06.062

Nomenclature

A	constants for analytical analysis
a, b, c	coefficients of series
C	oxygen concentration
D	diffusion coefficient
D_{bulk}	binary diffusion coefficient of O_2 and N_2
D_{eq}	equivalent diffusion coefficient
D_{eff}	effective diffusion coefficient
J	mass flux
l	porous sample thickness
L	channel length
M	constants for inverse-matrix analysis
Q	diffusion ratio
t	time
Δt_{expl}	critical time step for CFL condition
z	cell direction axis
Z	distance between the gate and the oxygen sensor

Greek Letters

α, β, ξ	variables, which are used for the simplification of the results
λ	eigen value
φ	interface oxygen concentration

Subscripts

1	Region 1
2	Region 2
i	position index
n	time index
k	summation index
p	porous region

Superscripts

n	time steps

boundary conditions is followed. To the authors' knowledge, there is no study found in literature that deals with nonhomogeneous case of diffusion media. This method allows a short, more compact experimental apparatus and provides greater accuracy through extended measurement times.

2. Experimental design

A simple sketch of this cell used is shown in Fig. 1. The half-length of the channel is 0.08 m and the inner diameter of the cell is 0.026 m. A ball valve is located between the two chambers and a Sigracet SGL 10AA porous sample was inserted in one chamber near the valve to investigate the effective diffusion coefficient. There is about 200 μm distance between the valve and the sample. To simplify the calculations; this gap is assumed to be on the lower side of the valve (in the first chamber); hence the distance between the valve and the porous sample is assumed to be zero.

For the experiments, first, the upper chamber of the cell is purged with a gas mixture of 90% nitrogen with 10% oxygen, whereas the lower chamber contains atmospheric air. After equilibrium is obtained and the homogeneity is observed, the initial oxygen content in both chambers is measured. Then, the valve between the chambers is opened to enable gas diffusion and the oxygen molecules diffuse from the lower chamber to the upper chamber. The dynamic O_2 concentration is measured and recorded for about three minutes with a measurement frequency of 2 Hz, by an Ocean Optics Neofox 1000 μm oxygen sensor, which is placed in the upper chamber, at a location of 13.5 mm from the valve.

The governing equation for mass transfer in the cell is "Fick's second law" and can be seen in Eq. (1).

$$\frac{\partial C}{\partial t} = D\frac{\partial^2 C}{\partial z^2} \tag{1}$$

In this equation, D becomes D_{eff} if the diffusion medium is porous. If the medium is open, then D becomes D_{bulk}. By using the measured concentration at the sensor point and the analytical solution of the Fick's second law, D_{eff}/D_{bulk} values are deduced.

Two different methods were used to obtain the analytical solution of the Fick's second law. First, the regular solution, which is called "the standard method" in the current study, was applied for the experiments. Then a new analytical solution, which is called "the new method" was utilized. This new solution method is introduced in Section 3,

For the case with the standard solution; the following equations (Refs. [4–9]) were applied and the effective diffusion coefficients were determined.

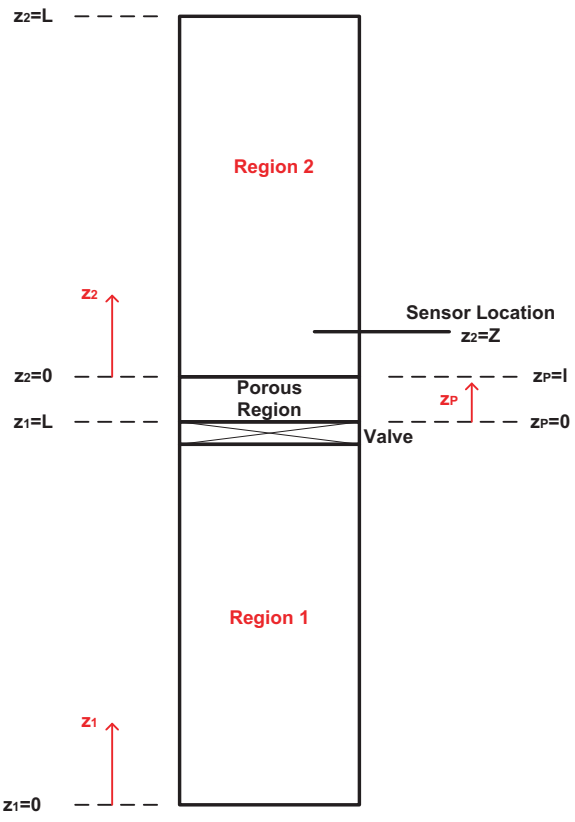

Fig. 1. A simple schematic of the Loschmidt diffusion cell.

$$D_{eq} = \frac{Z^2}{4\,t\,erfinv\left[\left(\frac{C_{1,0}-2C+C_{2,0}}{C_{1,0}-C_{2,0}}\right)^2\right]} \tag{2}$$

$$D_{eff} = \frac{l}{\frac{Z}{D_{eq}} - \frac{Z-l}{D_{bulk}}} \tag{3}$$

In these equations, D_{bulk} is defined as the binary gas diffusion coefficient and in this study; it represents the diffusion coefficient of O_2 and N_2 gases. D_{bulk} is assumed to be constant and it does not change with concentration, pressure, or temperature for simplification. D_{eff} is the effective diffusion coefficient of a gas pair in a porous medium. Z is the distance between oxygen sensor and the valve. $C_{1,0}$ and $C_{2,0}$ are the initial oxygen concentrations in the lower and upper chambers, respectively. D_{eq} is the equivalent diffusion coefficient of the layers. The detailed information about these parameters can be found in Refs. [4–9]. This study is focused on the new method.

Eqs. (2) and (3) can be applied under the assumption of infinite cell lengths. The assumption allows for constant boundary conditions equal to the initial chamber concentrations. It becomes invalid when the diffusion wave reaches the end of the chamber. Therefore, this assumption requires very long experimental apparatus, which is more costly. In the following section, a new analytical model is developed to eliminate this restricted boundary condition. The cells used in our testing were sufficiently long to enable use of this method for a period of time so that a comparison of approaches could be made.

The full governing equations, boundary conditions and the new method are explained in detail in the following section.

3. Analytical method

A new analytical method was developed to use a compact Loschmidt diffusion cell. The method is applied using finite boundary conditions; hence it enables a smaller cell length.

Fick's second law is used for concentrations in all three regions. Mass fluxes at $z = 0$ and $z = 2L + l$ are zero, since there is no mass transfer from or to the overall cell. Mass fluxes in all three regions can be defined as in Eqs. (4)–(6).

$$J_1 = -D\frac{\partial C_1}{\partial z} \tag{4}$$

$$J_p = -D_{eff}\frac{\partial C_p}{\partial z} \tag{5}$$

$$J_2 = -D\frac{\partial C_2}{\partial z} \tag{6}$$

The mass fluxes are equal to each other at the co-joined interfaces. Likewise, the concentrations are also as the same. All these related governing equations, boundary conditions, and the initial conditions are summarized for all three regions in Table 1. To solve the governing equations with the specified boundary conditions stated in Table 1, a combination of three different coordinate systems is used. These systems are also shown in Fig. 1. This new system is used to simplify the solution procedure, as it is more appropriate to apply the Fourier series when one of the boundary coordinates is zero.

There are several studies performed for the interface conditions between porous media. Crank [10], defined the interface condition between two media as "$C_1 = PC_2 + Q$" where P and Q are constants and 1 and 2 represent the first and second medium, respectively. If the continuity of concentration is assumed, then P and Q would be accepted as 1 and 0, respectively. Peters and Smith [14] have performed a numerical study on boundary and interface conditions for mass transport in a porous medium and they introduced three different interface conditions, which can be considered for the analysis; continuity of concentration, continuity of mass flux, and continuity of both concentration and mass flux. They concluded from the study that the third condition should be satisfied at the interface of two media. Leij et al. [15] investigated a one dimensional solute transport in a layered soil profile. They analyzed all three interface conditions and concluded as the most realistic result is that with the continuity of both concentration and mass flux at the interfaces. The authors found a relative error of less than 0.1% when they imposed both conditions.

In this study, continuity of both concentration and mass flux are assumed as the interface conditions. The solutions for all three regions are shown in the following sections.

Table 1
Fick's second law applied to the system shown in Fig. 1.

Regions	Governing equations	Boundary conditions	Initial conditions
1	$D\frac{\partial^2 C_1(z,t)}{\partial z^2} = \frac{\partial C_1(z,t)}{\partial t}$	$\frac{\partial C_1(0,t)}{\partial z} = 0$ $J_1(L,t) = J_p(L,t)$ $C_1(L,t) = C_p(L,t)$	$C_1(z,0) = C_{1,0}$
Porous	$D_{eff}\frac{\partial^2 C_p(z,t)}{\partial z^2} = \frac{\partial C_p(z,t)}{\partial t}$	$J_p(L,t) = J_1(L,t)$ $C_p(L,t) = C_1(L,t)$ $J_p(L+d,t) = J_2(L+d,t)$ $C_p(L+d,t) = C_2(L+d,t)$	$C_p(z,0) = C_{2,0}$
2	$D\frac{\partial^2 C_2(z,t)}{\partial z^2} = \frac{\partial C_2(z,t)}{\partial t}$	$\frac{\partial C_2(2L+d,t)}{\partial z} = 0$ $J_2(L+d,t) = J_p(L+d,t)$ $C_2(L+d,t) = C_p(L+d,t)$	$C_2(z,0) = C_{2,0}$

3.1. Region 1

For the analytical analysis of the mass transport in Region 1 (Fig. 1), the governing equation for concentration distribution and the related boundary and initial conditions are written in Eqs. (7), (8), and (9), respectively.

$$\frac{\partial C_1(z_1,t)}{\partial t} = D\frac{\partial^2 C_1(z_1,t)}{\partial z_1^2} \tag{7}$$

$$\frac{\partial C_1(0,t)}{\partial z_1} = 0 \tag{8a}$$

$$C_1(z_1 = L,t) = C_p(z_p = 0,t) = \varphi_1(t)\ \text{(any time-dependent variable)} \tag{8b}$$

$$C_1(z_1,0) = C_{1,0} \tag{9}$$

Separation of variables cannot be used here, since the boundary conditions are not zero. Then, the solution must be divided into two parts; homogeneous solution and deviation from homogeneity. The summation of the two parts will be the final solution.

$$C_1(z_1,t) = [C_1(z_1,t)]_h + [C_1(z_1,t)]_d \tag{10}$$

For the homogeneous part, the following condition is assumed.

$$[C_1(z_1,t)]_h = A_1(t)z_1 + A_2(t) \tag{11}$$

where $A_1(t)$ and $A_2(t)$ are time-dependent variables. When, the boundary conditions stated in Eq. (8) applied to Eq. (11), the following equation is obtained.

$$[C_1(z,t)]_h = \varphi_1(t) \tag{12}$$

Fick's second law and the related boundary and initial conditions are stated for the deviation from homogeneity part of the solution as shown in Eqs. (13), (14), and (15), respectively.

$$\frac{\partial[C_1(z_1,t)]_d}{\partial t} = D\frac{\partial^2[C_1(z_1,t)]_d}{\partial z_1^2} \tag{13}$$

$$\frac{\partial[C_1(0,t)]_d}{\partial z_1} = 0 \tag{14a}$$

$$[C_1(L,t)]_d = 0 \tag{14b}$$

$$[C_1(z_1,0)]_d = C_{1,0} - \varphi_1(t) \tag{15}$$

Now, the separation of variables method can be applied to Eq. (13).

$$[C_1(z_1,t)]_d = \phi(z_1)T(t) \tag{16}$$

In this equation, the concentration is separated into two functions, $\Phi(z_1)$ and $T(t)$, where $\Phi(z_1)$ is only a function of position and $T(t)$ is just time-dependent. After applying the separation of variables technique, the following general solutions for $\Phi(z_1)$ and $T(t)$ are obtained:

$$T(t) = A_3 e^{-\lambda^2 Dt} \tag{17}$$

$$\phi(z_1) = A_4\cos(\lambda z_1) + A_5\sin(\lambda z_1) \tag{18}$$

where λ is any constant here. The new forms of the boundary conditions are shown in Eq. (19).

$$C'(0,t) = \phi'(0)T(t) = 0 \quad \therefore \phi'(0) = 0 \tag{19a}$$

$$C(L,t) = \phi(L)T(t) = 0 \quad \therefore \phi(L) = 0 \tag{19b}$$

After the first derivative of Φ is obtained and Eq. (19a) is applied, A_5 becomes zero and the following result is obtained:

$$\phi(z_1) = A_4\cos(\lambda z_1) \tag{20}$$

Now, Eq. (19b) must be applied to Eq. (20).

$$\phi(L) = A_4\cos(\lambda L) = 0 \quad \therefore \cos(\lambda L) = 0 \tag{21}$$

Hence;

$$\lambda_{1,k} = \frac{(2k+1)\pi}{2L} \quad (k = 0,1,2,3,\ldots) \tag{22}$$

Combining Eqs. (21) and (17), the deviation part of the concentration equation is obtained as follows.

$$[C_1(z_1,t)]_d = \sum_{k=0}^{\infty} a_k e^{-\lambda_{1,k}^2 Dt}\cos(\lambda_{1,k} z_1) \tag{23}$$

There is still an unknown left in Eq. (23). To find a_k, the Fourier cosine expansion and the initial condition stated in Eq. (15) must be used.

$$a_k = \frac{2}{L}\int_0^L [C_{1,0} - \varphi_1(t)]\cos(\lambda_{1,k} z_1)dz \tag{24}$$

$$a_k = \frac{2[C_{1,0} - \varphi_1(t)]}{L\lambda_{1,k}}(-1)^k \tag{25}$$

Finally, inserting Eqs. (23), (25), and (12) into Eq. (10), the concentration distribution formula for the first region can be obtained:

$$C_1(z_1,t) = \varphi_1(t) + 4[C_{1,0} - \varphi_1(t)]\sum_{k=0}^{\infty}\frac{(-1)^k}{(2k+1)\pi}e^{-\left[\frac{(2k+1)\pi}{2L}\right]^2 Dt} \times \cos\left(\frac{(2k+1)\pi}{2L}z_1\right) \tag{26}$$

where $\varphi_1(t)$ is the time-dependent gas concentration at the interface between the first region and the porous sample and will be determined as shown later by using equal mass flux interface condition.

3.2. Porous region

To analyze the mass transfer in the Region P in Fig. 1, Fick's second law and the related boundary and initial conditions are written in Eqs. (27), (28), and (29), respectively.

$$\frac{\partial C_p(z_p,t)}{\partial t} = D_{eff}\frac{\partial^2 C_p(z_p,t)}{\partial z_p^2} \tag{27}$$

$$C_p(z_p = 0,t) = C_1(z_1 = L,t) = \varphi_1(t) \tag{28a}$$

$$C_p(z_p = l,t) = C_2(z_2 = 0,t) = \varphi_2(t) \tag{28b}$$

$$C_p(z_p,0) = C_{2,0} \tag{29}$$

As with the case in the first region, separation of variables cannot be used here, since the boundary conditions are nonhomogeneous. The procedure is the same as that for Region 1.

$$C_p(z_p,t) = [C_p(z_p,t)]_h + [C_p(z_p,t)]_d \tag{30}$$

For the homogeneous part, the following assumption is used.

$$[C_p(z_p,t)]_h = A_6(t)z_p + A_7(t) \tag{31}$$

where $A_6(t)$ and $A_7(t)$ are time-dependent variables. To have the particular solution, the boundary conditions, which are stated in Eq. (28), must be applied to Eq. (31). The homogeneous solution is found as in Eq. (32).

$$[C_p(l,t)]_h = \frac{[\varphi_2(t) - \varphi_1(t)]}{l}z_p + \varphi_1(t) \tag{32}$$

For deviation from homogeneity, the following governing equation for the concentration and the related boundary and initial conditions are used.

$$\frac{\partial[C_p(z_p,t)]_d}{\partial t} = D_{eff}\frac{\partial^2[C_p(z_p,t)]_d}{\partial z_p^2} \tag{33}$$

$$[C_p(0,t)]_d = 0 \tag{34a}$$

$$[C_p(l,t)]_d = 0 \tag{34b}$$

$$C_p(z_p,0) = C_{2,0} - \frac{[\varphi_2(t) - \varphi_1(t)]}{l}z_p - \varphi_1(t) \tag{35}$$

Separation of variables can be applied to Eq. (35) to find the general solution. As the previous two separation-of-variables methods used in this study, the following conditions are obtained.

$$[C_p(z_p,t)]_d = \phi(z_p)T(t) \tag{36}$$

$$T(t) = A_8 e^{-\lambda^2 D_{eff}t} \tag{37}$$

$$\phi(z_p) = A_9\cos(\lambda z_p) + A_{10}\sin(\lambda z_p) \tag{38}$$

Furthermore, the boundary conditions are shown below.

$$[C_p(0,t)]_d = \phi(0)T(t) = 0 \quad \therefore \phi(0) = 0 \tag{39a}$$

$$[C_p(l,t)]_d = \phi(l)T(t) = 0 \quad \therefore \phi(l) = 0 \tag{39b}$$

Eq. (39) are used to find the particular non-homogeneous solution (Eq. (40)).

$$[C_p(z_p,t)]_d = \sum_{k=0}^{\infty} b_k e^{-\lambda_{p,k}^2 D_{eff}t}\sin(\lambda_{p,k} z_p) \tag{40}$$

$$\lambda_{p,k} = \frac{k\pi}{l} \quad (k = 0,1,2,3,\ldots) \tag{41}$$

The initial condition and the Fourier sine expansion must be used to obtain b_k in Eq. (40).

$$b_k = \frac{2}{l}\int_0^d \left[C_{2,0} - \frac{[\varphi_2(t)-\varphi_1(t)]}{l} z_p - \varphi_1(t)\right] \sin(\lambda_{p,k} z_p) dz \tag{42}$$

$$b_k = \frac{2[[C_{2,0}-\varphi_1(t)][1-(-1)^k] + [\varphi_2(t)-\varphi_1(t)](-1)^k]}{l\lambda_{p,k}} \tag{43}$$

Finally, the full concentration solution in the porous region can be determined by combining the Eqs. (32) and (40).

$$C_p(z_p,t) = \frac{[\varphi_2(t)-\varphi_1(t)]}{l} z_p + \varphi_1(t) + \sum_{k=0}^{\infty} b_k e^{-\lambda_{p,k}^2 D_{eff} t} \sin(\lambda_{p,k} z_p) \tag{44}$$

where, b_k and $\lambda_{p,k}$ are defined in Eqs. (43) and (41), respectively. $\varphi_2(t)$ is the time-dependent gas concentration at the interface between the second region and the porous sample and can be determined simultaneously with $\varphi_1(t)$ using equal mass flux interface condition, as shown later in the text.

3.3. Region 2

The governing equation for the concentration distribution and the related boundary and initial conditions for Region 2 (Fig. 1) are stated in Eqs. (45), (46), and (47), respectively.

$$\frac{\partial C_2(z_2,t)}{\partial t} = D\frac{\partial^2 C_2(z_2,t)}{\partial z_2^2} \tag{45}$$

$$C_2(z_2=0,t) = C_p(z_p=l,t) = \varphi_2(t) \tag{46a}$$

$$\frac{\partial C_2(L,t)}{\partial z_2} = 0 \tag{46b}$$

$$C_2(z_2,0) = C_{2,0} \tag{47}$$

As in two previous cases; the solution must be divided into two parts; homogeneous solution and the deviation from homogeneity (or nonhomogeneous solution).

$$C_2(z_2,t) = [C_2(z_2,t)]_h + [C_2(z_2,t)]_d \tag{48}$$

The following assumption is made for the solution of the homogeneous part.

$$[C_2(z_2,t)]_h = A_{11}(t) z_2 + A_{12}(t) \tag{49}$$

where $A_{11}(t)$ and $A_{12}(t)$ are time-dependent variables. Hence, the boundary conditions stated in Eq. (46) can be applied to Eq. (49). The homogeneous part of the solution can be stated as in Eq. (50).

$$[C_2(z_2,t)]_h = \varphi_2(t) \tag{50}$$

For the nonhomogeneous part of the solution, Fick's second law and the related boundary and initial conditions are stated in Eqs. (51), (52), and (53), respectively.

$$\frac{\partial [C_2(z_2,t)]_d}{\partial t} = D\frac{\partial^2 [C_2(z_2,t)]_d}{\partial z_2^2} \tag{51}$$

$$[C_2(0,t)]_d = 0 \tag{52a}$$

$$\frac{\partial [C_2(L,t)]_d}{\partial z_2} = 0 \tag{52b}$$

$$[C_2(z_2,0)]_d = C_{2,0} - \varphi_2(t) \tag{53}$$

Now, the separation of variables method can be applied to Eq. (51) to find the general solution.

$$[C_2(z_2,t)]_d = \phi(z_2) T(t) \tag{54}$$

The solutions can be stated as follows.

$$T(t) = A_{13} e^{-\lambda^2 D t} \tag{55}$$

$$\phi(z_2) = A_{14}\cos(\lambda z_2) + A_{15}\sin(\lambda z_2) \tag{56}$$

By using Eq. (54), the boundary conditions can be restated as follows.

$$C_2(0,t) = \phi(0)T(t) = 0 \quad \therefore \phi(0) = 0 \tag{57a}$$

$$C_2'(L,t) = \phi'(L)T(t) = 0 \quad \therefore \phi'(L) = 0 \tag{57b}$$

Eq. (58) is obtained after applying the boundary conditions, which are stated in Eq. (52).

$$[C_2(z_2,t)]_d = \sum_{k=0}^{\infty} c_k e^{-\lambda_{2,k}^2 D t} \sin(\lambda_{2,k} z_2) \tag{58}$$

$$\lambda_{2,k} = \frac{(2k+1)\pi}{2L} \quad (k = 0,1,2,3,\ldots) \tag{59}$$

To find c_k, the Fourier cosine expansion and the initial condition stated in Eq. (53) must be used.

$$c_k = \frac{2}{L}\int_0^L [C_{2,0} - \varphi_2(t)] \sin(\lambda_{2,k} z_2) dz \tag{60}$$

$$c_k = \frac{2[C_{2,0}-\varphi_2(t)]}{L\lambda_{2,k}} \tag{61}$$

Finally, the concentration distribution for the second region can be obtained by inserting Eqs. (58), (59), (61) and (50) into Eq. (48),

$$C_2(z_2,t) = \varphi_2(t) + 4[C_{2,0}-\varphi_2(t)]\sum_{k=0}^{\infty} \frac{1}{(2k+1)\pi} e^{-\left[\frac{(2k+1)\pi}{2L}\right]^2 D t} \times \sin\left(\frac{(2k+1)\pi}{2L} z_1\right) \tag{62}$$

Before the determination of interfacial concentrations, $\varphi_1(t)$ and $\varphi_2(t)$, the following results are summarized below.

$$C_1(z_1,t) = \varphi_1(t) + \frac{2[C_{1,0}-\varphi_1(t)]}{L}\alpha_1(z_1,t) \tag{63}$$

$$C_2(z_2,t) = \varphi_2(t) + \frac{2[C_{2,0}-\varphi_2(t)]}{L}\alpha_2(z_2,t) \tag{64}$$

$$C_p(z_p,t) = \frac{[\varphi_2(t)-\varphi_1(t)]}{l} z_p + \varphi_1(t) + \frac{2[C_{2,0}-\varphi_1(t)]}{l}\alpha_3(z_p,t) + \frac{2[\varphi_2(t)-\varphi_1(t)]}{l}\alpha_4(z_p,t) \tag{65}$$

where,

$$\alpha_1(z_1,t) = \sum_{k=0}^{\infty} \frac{2L(-1)^k}{(2k+1)\pi} e^{-\left[\frac{(2k+1)\pi}{2L}\right]^2 D t} \cos\left(\frac{(2k+1)\pi}{2L} z_1\right) \tag{66}$$

$$\alpha_2(z_2,t) = \sum_{k=0}^{\infty} \frac{2L}{(2k+1)\pi} e^{-\left[\frac{(2k+1)\pi}{2L}\right]^2 D t} \sin\left(\frac{(2k+1)\pi}{2L} z_1\right) \tag{67}$$

$$\alpha_3(z_p,t) = \sum_{k=1}^{\infty} \frac{[1-(-1)^k]l}{k\pi} e^{-\left[\frac{k\pi}{l}\right]^2 D_{eff} t} \sin\left(\frac{k\pi}{l} z_p\right) \tag{68}$$

$$\alpha_4(z_p,t) = \sum_{k=1}^{\infty} \frac{(-1)^k l}{k\pi} e^{-\left[\frac{k\pi}{l}\right]^2 D_{eff} t} \sin\left(\frac{k\pi}{l} z_p\right) \tag{69}$$

Concentrations at the interfaces can be determined by using the interface conditions stated below:

$$J_1(z_1 = L,t) = J_p(z_p = 0,t) \tag{70}$$

$$J_2(z_2 = 0,t) = J_p(z_p = l,t) \tag{71}$$

where, J_1, J_p, and J_2 are mass fluxes and they are defined in Eqs. (5)–(7), respectively. Using Eqs. (63)–(71), the interface concentrations can be determined as follows:

$$\varphi_1 = \frac{C_{1,0}C_{2,0}(\xi_1+\xi_2+\xi_3)}{C_{2,0}\xi_1 + C_{1,0}(\xi_2+\xi_3)} \tag{72}$$

$$\varphi_2 = \frac{C_{1,0}C_{2,0}(\xi_2+\xi_3+\xi_4+\xi_5)}{C_{2,0}\xi_1 + C_{1,0}(\xi_2+\xi_3)} \tag{73}$$

where;

$$\xi_1 = \beta_1 C_{1,0} lD[2\beta_4 dD + (1+2\beta_6)LD_{eff}] \tag{74}$$

$$\xi_2 = LlC_{2,0}\beta_4 DD_{eff}(1+2\beta_2+2\beta_3) \tag{75}$$

$$\xi_3 = C_{2,0}L^2 D_{eff}^2(\beta_2-\beta_5-2\beta_3\beta_5+2\beta_2\beta_6) \tag{76}$$

$$\xi_4 = 2\beta_1\beta_4 C_{2,0} l^2 D^2 \tag{77}$$

$$\xi_5 = \beta_1 lDLD_{eff}[C_{1,0}(1+2\beta_5+2\beta_6) - 2\beta_5 C_{2,0}] \tag{78}$$

$$\beta_1(t) = \sum_{k=0}^{\infty}(-1)^{2k} e^{-\left[\frac{(2k+1)\pi}{2L}\right]^2 Dt} \tag{79}$$

$$\beta_2(t) = \sum_{k=1}^{\infty}[1-(-1)^k] e^{-\left[\frac{k\pi}{l}\right]^2 D_{eff}t} \tag{80}$$

$$\beta_3(t) = \sum_{k=1}^{\infty}(-1)^k e^{-\left[\frac{k\pi}{l}\right]^2 D_{eff}t} \tag{81}$$

$$\beta_4(t) = \sum_{k=0}^{\infty} e^{-\left[\frac{(2k+1)\pi}{2L}\right]^2 Dt} \tag{82}$$

$$\beta_5(t) = \sum_{k=1}^{\infty}[1-(-1)^k] e^{-\left[\frac{k\pi}{l}\right]^2 D_{eff}t} \tag{83}$$

$$\beta_6(t) = \sum_{k=1}^{\infty}(-1)^{2k} e^{-\left[\frac{k\pi}{l}\right]^2 D_{eff}t} \tag{84}$$

4. Numerical methods

4.1. Inverse-matrix

To prove the analytical solution, the inverse-matrix method was used to find the concentration distribution throughout the Loschmidt cell. This method is an implicit one and to find the nodal equations, the finite difference approach is used. In this study, i represents the node number in z-direction and n represents the time steps. First, the system domain must be discretized. In Fig. 2, the cell is divided into twelve pieces, and thirteen nodes for a very simple demonstration.

Table 1 summarizes the governing equations and boundary and initial conditions, which must be used for this problem. For Regions 1 and 2, the governing equation for the concentration distribution can be seen in Eq. (3). This equation is valid for the nodes 2, 3, 4, 10, 11, and 12. For left hand side (LHS) of Eq. (85), the forward-difference is applied whereas for the RHS, the central-difference is performed. Then, the nodal equation become as follows:

$$C(i,n) = \left(-\frac{D\Delta t}{\Delta z^2}\right)C(i-1,n+1) + \left(1+\frac{2D\Delta t}{\Delta z^2}\right)C(i,n+1) + \left(-\frac{D\Delta t}{\Delta z^2}\right)C(i+1,n+1) \tag{85}$$

For the porous region, the following equation is used for the concentration distribution.

$$\frac{\partial C(z,t)}{\partial t} = D_{eff}\frac{\partial^2 C(z,t)}{\partial z^2} \tag{86}$$

Eq. (86) is valid for the nodes 6, 7, and 8. The nodal equation is determined as follows.

$$C(i,n) = \left(-\frac{D\Delta t}{\Delta z_p^2}\right)C(i-1,n+1) + \left(1+\frac{2D\Delta t}{\Delta z_p^2}\right)C(i,n+1) + \left(-\frac{D\Delta t}{\Delta z_p^2}\right)C(i+1,n+1) \tag{87}$$

For the first node, the boundary condition, which is stated in Eq. (88) can be used and the forward difference can be applied to find the nodal equation.

$$\frac{\partial C(0,t)}{\partial z} = 0 \tag{88}$$

$$C(2,n+1) - C(1,n+1) = 0 \tag{89}$$

For the last node, the boundary condition, which is stated in Eq. (90) can be used and the backward difference can be applied to find the nodal equation.

$$\frac{\partial C(2L+l,t)}{\partial z} = 0 \tag{90}$$

$$C(13,n+1) - C(12,n+1) = 0 \tag{91}$$

For the fifth node, the boundary condition stated in Eq. (92) is used and the nodal equation is written below.

$$D\frac{\partial C}{\partial z} = D_{eff}\frac{\partial C_p}{\partial z} \tag{92}$$

$$-\frac{D}{\Delta z}C(4,n+1) + \left(\frac{D}{\Delta z}+\frac{D_{eff}}{\Delta z_p}\right)C(5,n+1) - \frac{D_{eff}}{\Delta z_p}C(6,n+1) = 0 \tag{93}$$

Finally, for the ninth node, the boundary condition stated in Eq. (94) is used. The derivation of the nodal equation is written below.

$$D_{eff}\frac{\partial C_p}{\partial z} = D\frac{\partial C}{\partial z} \tag{94}$$

$$-\frac{D_{eff}}{\Delta z_p}C(8,n+1) + \left(\frac{D}{\Delta z}+\frac{D_{eff}}{\Delta z_p}\right)C(9,n+1) - \frac{D}{\Delta z}C(10,n+1) = 0 \tag{95}$$

These equations for all nodes and for the first time step can be written in a matrix form as in Fig. 3. The initial conditions are defined in Table 1. All the parameters in the matrix are shown below:

$$M_1 = -\frac{D\Delta t}{\Delta z^2}, \quad M_2 = 1-2M_1, \quad M_3 = -\frac{D_{eff}\Delta t}{\Delta z_p^2}, \quad M_4 = 1-2M_3$$
$$M_5 = -\frac{D}{\Delta z}, \quad M_6 = -\frac{D_{eff}}{\Delta z_p}, \quad M_7 = -M_5 - M_6 \tag{96}$$

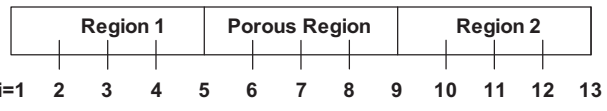

Fig. 2. A simple demonstration of a mesh generation for the finite-difference solution.

The left part of the left hand side of the matrix is the coefficient matrix and can be indicated by $[B]$. The right part of the LHS is the unknown vector and can be indicated by $[C]$. Finally, the RHS is the result vector and labeled as $[R]$. Then, this equation can be written as in Eq. (97).

$$[B][C] = [R] \tag{97}$$

To find the individual concentrations at the nodes, the inverse of the matrix B must be multiplied by both sides.

$$[C] = inv[B] \cdot [R] \tag{98}$$

The total node number was increased to 1000 spatial nodes in this analysis to improve accuracy.

4.2. The finite volume discretization

A finite volume discretization was also applied to the diffusion problem to test the accuracy of the new analytical solution. Again, Fick's law was applied in one dimension and the domain was discretized. A simple mesh is shown in Fig. 4. Seven and six nodes were used during derivation for mass concentration and mass flux, respectively. Four Thousand nodes were used during the actual computational runs.

The governing equation for diffusion can be modified as follows:

$$\frac{\partial C}{\partial t} + \frac{\partial F}{\partial z} = 0 \tag{99}$$

where F represents the mass flux and can be defined as Eq. (100).

$$F = -D\frac{\partial C}{\partial z} \tag{100}$$

At the boundaries, fluxes are zero and the initial conditions are the same as the previous sections.

The nodal equations for the fluxes must be derived for all nodes in Fig. 4. For internal nodes, the following nodal equations are obtained.

$$F_i^n = -D\frac{(C_{i+1}^n - C_i^n)}{\Delta z} \tag{101}$$

In this equation, D represents D_{eff} if the node is in porous region; otherwise it is equal to D_{bulk} and n stands for time steps. i is the node number in z-direction. For the first and the last nodes, the fluxes are zero due to the boundary conditions.

$$F_1^n = F_6^n = 0 \tag{102}$$

For mass concentration, the nodal equations for the internal nodes can be written as follows:

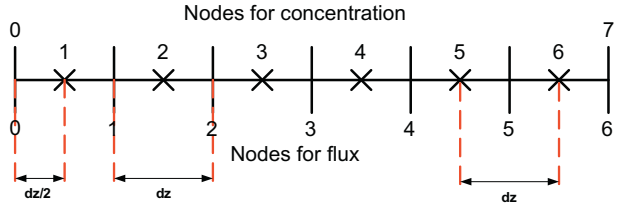

Fig. 4. A simple control volume in one dimension for finite volume analysis.

$$C_i^{n+1} = C_i^n - \frac{\Delta t}{\Delta z}(F_i^n - F_{i-1}^n) \tag{103}$$

Since the fluxes are zero at the boundaries, the following equations were determined for the boundary nodes.

$$C_0^n = C_1^n, \quad C_7^n = C_6^n \tag{104}$$

Super time stepping (STS) acceleration is used for time steps in this analysis. The STS technique is used for speeding up the explicit time-stepping schemes for parabolic problems. More information can be found in Refs. [16,17].

To utilize this method, first Δt_{expl}, which is the critical time step, should be determined by using Courant–Friedrichs–Lewy (CFL) criterion [13,16,17]. The CFL condition for the problem can be determined if the fluxes in Eq. (103) are written in their open form, Eq. (101). After further manipulations, the CFL condition is found as written in Eq. (105).

$$\Delta t_{expl} \leqslant \frac{\Delta z^2}{2D} \tag{105}$$

Super-time-stepping can now be utilized but before this, four new STS parameters must be introduced. ΔT is defined as a super-step, which consists of sub-steps denoted by τ_i, where $i = 1,2,\ldots,N$. Another parameter, μ, can be defined as $4D/\Delta z^2$. Finally, ν is any number between μ_{min} and μ_{max} which is referred to as the damping factor [15]. Then, the following equation is used to determine the sub-steps:

$$\tau_i = \Delta t_{expl}\left((\nu-1)\cos\left(\frac{2i-1}{N}\frac{\pi}{2}\right) + \nu + 1\right)^{-1}, \quad \text{where } i = 1,2,\ldots,N \tag{106}$$

Hence, the super-time-step becomes:

$$\Delta T = \sum_{i=1}^{N} \tau_i \tag{107}$$

Analysis for STS parameters can be found in Refs. [15,16]. For the current study, this technique is used to reduce the run-time of

$$\begin{vmatrix}
1 & -1 & 0 & 0 & 0 & 0 & 0 & 0 & 0 & 0 & 0 & 0 & 0 \\
M_1 & M_2 & M_1 & 0 & 0 & 0 & 0 & 0 & 0 & 0 & 0 & 0 & 0 \\
0 & M_1 & M_2 & M_1 & 0 & 0 & 0 & 0 & 0 & 0 & 0 & 0 & 0 \\
0 & 0 & M_1 & M_2 & M_1 & 0 & 0 & 0 & 0 & 0 & 0 & 0 & 0 \\
0 & 0 & 0 & M_5 & M_7 & M_6 & 0 & 0 & 0 & 0 & 0 & 0 & 0 \\
0 & 0 & 0 & 0 & M_3 & M_4 & M_3 & 0 & 0 & 0 & 0 & 0 & 0 \\
0 & 0 & 0 & 0 & 0 & M_3 & M_4 & M_3 & 0 & 0 & 0 & 0 & 0 \\
0 & 0 & 0 & 0 & 0 & 0 & M_3 & M_4 & M_3 & 0 & 0 & 0 & 0 \\
0 & 0 & 0 & 0 & 0 & 0 & 0 & M_6 & M_7 & M_5 & 0 & 0 & 0 \\
0 & 0 & 0 & 0 & 0 & 0 & 0 & 0 & M_1 & M_2 & M_1 & 0 & 0 \\
0 & 0 & 0 & 0 & 0 & 0 & 0 & 0 & 0 & M_1 & M_2 & M_1 & 0 \\
0 & 0 & 0 & 0 & 0 & 0 & 0 & 0 & 0 & 0 & M_1 & M_2 & M_1 \\
0 & 0 & 0 & 0 & 0 & 0 & 0 & 0 & 0 & 0 & 0 & -1 & 1
\end{vmatrix}
\begin{vmatrix} C(1,2) \\ C(2,2) \\ C(3,2) \\ C(4,2) \\ C(5,2) \\ C(6,2) \\ C(7,2) \\ C(8,2) \\ C(9,2) \\ C(10,2) \\ C(11,2) \\ C(12,2) \\ C(13,2) \end{vmatrix}
= \begin{vmatrix} 0 \\ C_{10} \\ C_{10} \\ C_{10} \\ 0 \\ C_{20} \\ C_{20} \\ C_{20} \\ 0 \\ C_{20} \\ C_{20} \\ C_{20} \\ 0 \end{vmatrix}$$

Fig. 3. Nodal equations in matrix form for the diffusion problem.

the C++ code, which was used to solve the problem with finite volume discretization.

5. Results and discussion

Both numerical and analytical solution techniques were applied to the diffusion problem in a Loschmidt cell with a porous layer. The effective diffusion coefficient was taken as an average literature value of 6.0E−6 m^2/s and the binary diffusion coefficient of O_2 and N_2 gases was taken as 1.76E−5 m^2/s (Ref. [2, p. 212]). The total cell length was 0.1604 m and 0.0004 m of this length was occupied by the porous sample. This porous sample was located at the middle of the cell. The initial O_2 mole fractions in the simulations were 0.2 for the left chamber, and 0.1 for the porous part and the right chamber.

Fig. 5 is a plot of the predicted oxygen concentration in a Loschmidt cell with a porous layer after 1, 10, and 20 s. It can be seen from all three figures that there is a strong overlap between the numerical and analytical solutions. When, time increases, the oxygen gas in the first cell diffuses through the porous sample, and to the second chamber.

In Fig. 6, the analytical solution after 1000 s is plotted. It can be seen in the figure that the oxygen concentration reaches equilibrium

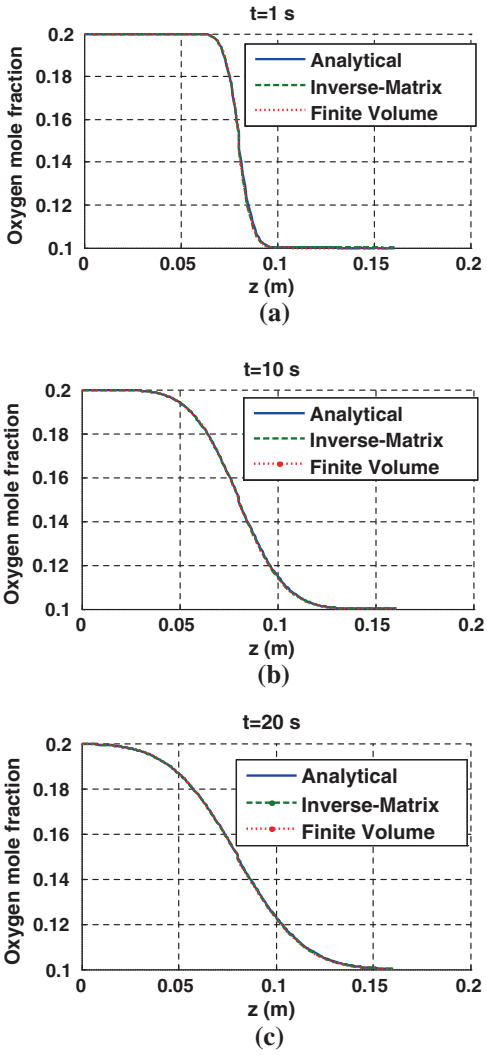

Fig. 5. Oxygen mole fraction calculated by three different methods in Loschmidt diffusion cell (a) t = 1 s, (b) t = 10 s, and (c) t = 20 s.

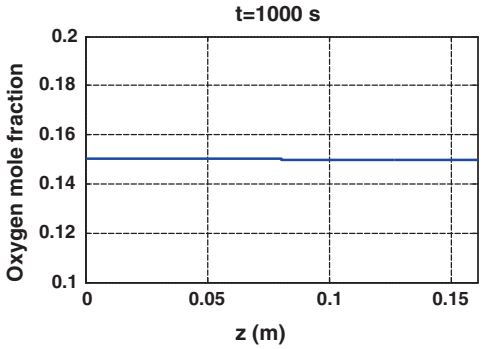

Fig. 6. Analytical solution at t = 1000 s.

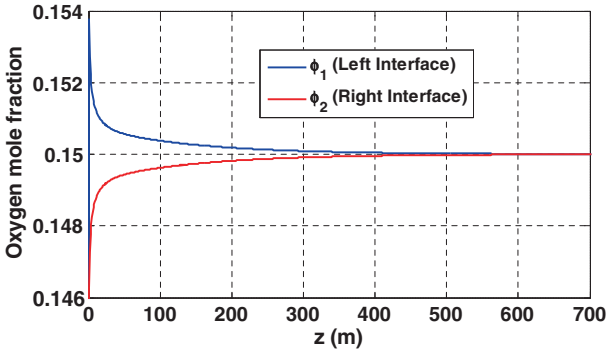

Fig. 7. O_2 concentrations at the interfaces between porous layer and the chambers.

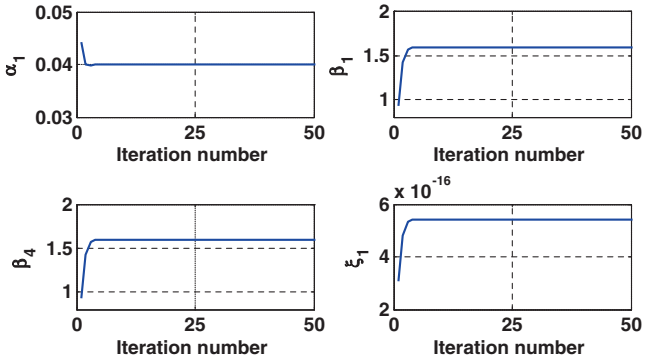

Fig. 8. Numerical results of the summations α_1, β_1, β_4, ξ_1 versus the iteration number.

throughout the cell as expected. In Fig. 7, the O_2 concentrations at both interfaces between the porous layer and the chambers are plotted within a time limit of 0 and 700 s. After about 600 s, there is no diffusion observed in the porous sample.

The two methods discussed in previous sections were used to determine D_{eff}. If the regular method is used, the effective diffusion coefficient can be determined directly by Eq. (2). However, in the results of the new method, there are several terms under summation. To simplify these terms, the results of each are calculated for several results and plotted against iteration number. Four of the results are shown in Fig. 8. As seen in the figure, approximately after the 10th iteration, the results do not change. To achieve high accuracy results, the code is terminated when the relative error between the consecutive values of the iterations becomes less than 1E−6.

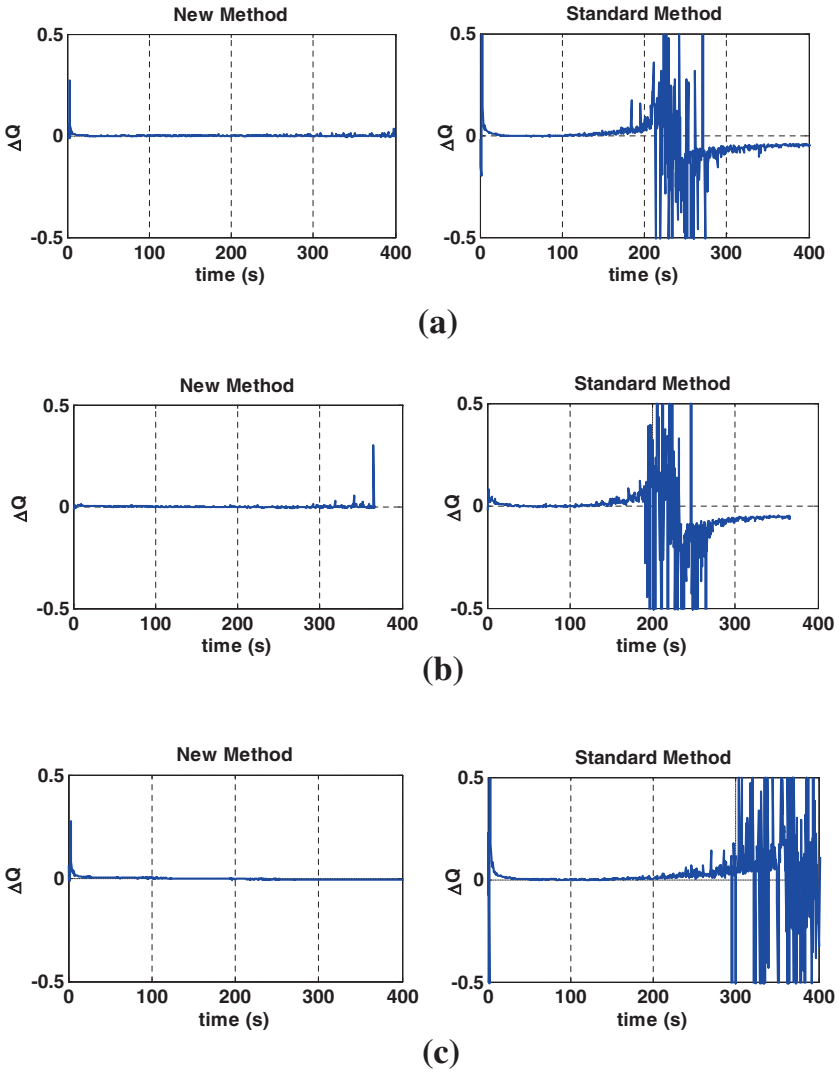

Fig. 9. Diffusion ratio of O_2 and N_2 through a dry 400 μm-thick-SGL10AA sample, normalized by Q_{mean}. Two different methods used with three different experimental data are shown in (a–c).

In the experiments, oxygen sensor is located in a place in the right chamber, where Eq. (64) represents the concentration. To determine D_{eff}, the following manipulation is used.

$$\varphi_2(t) - C_2(z_2,t) + \frac{2[C_{2,0} - \varphi_2(t)]}{L}\alpha_2(z_2,t) = f(z_2,t,D,D_{eff},L) \tag{108}$$

In this equation, C_2 is measured at the sensor point and all z_2 values are written as the sensor location. f must be zero for the correct D_{eff} value. To find D_{eff}, the following procedure is followed:

Several D_{eff} values are tried to yield Eq. (108). To do this, a wide scan between 10^{-8} and 10^{-4} with a step of 10^{-8} is used. When f becomes 0, the code ends and the correct D_{eff} value is determined. In other words, the final result for D_{eff} is determined where the right hand side-function intersects the D_{eff}-axis.

In Fig. 9, three different experimental results are shown. The cell internal geometry is as the same as in the numerical studies. As a porous sample, Sigracet SGL 10AA is used. Q is defined as the ratio of effective and bulk diffusion coefficients and Q_m is the mean value, which is calculated by a weighted approach, where the outliers are not included. Hence the deviation can be defined as follows:

$$\Delta Q(z,t) = Q_m - Q(z,t) \tag{109}$$

One way to compare the consistency and stability of each mathematical model is to plot the deviation in diffusion ratio with respect to time. In all figures, some initial instability is seen. This may be a result of the sliding effects of the valve.

The graphs on the left side of Fig. 9 show the calculations performed by using the new method, whereas the right hand side graphs are the results of the standard method. It can be seen that the new method provides more experimental time while enabling a compact diffusion cell with more stable results.

6. Conclusions

In this study, a new analytical approach is introduced and numerically verified for the Loschmidt diffusion cell which enables design and use of a more compact cell and a longer measurement time. A full analytical solution of Fick's second law of diffusion without infinite-cell-length assumption is performed. This new method is confirmed by two different numerical methods and it is concluded that it provides more experimental time with a more compact Loschmidt cell design. A future study can include the

gravitational effects to allow for different orientations of the test system.

7. Disclaimer

This report was prepared as an account of work sponsored by an agency of the United States Government. Neither the United States Government nor any agency thereof, nor any of their employees, makes any warranty, express or implied, or assumes any legal liability or responsibility for the accuracy, completeness, or usefulness of any information, apparatus, product, or process disclosed, or represents that its use would not infringe privately owned rights. Reference herein to any specific commercial product, process, or service by trade name, trademark, manufacturer, or otherwise does not necessarily constitute or imply its endorsement, recommendation, or favoring by the United States Government or any agency thereof.

Acknowledgments

This material is based upon work supported by the Department of Energy under Award Number DE-EE0000470.

Appendix A. Uncertainty analysis

Total experimental uncertainty of Q can be calculated as follows:

$$u_Q = \sqrt{um_{i=1}^{n}\left(\frac{\partial Q}{\partial x_i}u_i\right)^2} \tag{110}$$

where, x is any measured value and u is the related uncertainty.

In the current study, one of the most significant sources of error is the sensor sensitivity. The related uncertainty can be calculated below by using two different measurements under the same conditions. In this experiment, the measured parameters are concentrations and $u = \delta C$ is the uncertainty of the 300-μm oxygen probe.

$$\frac{\partial Q}{\partial C}\delta C = \frac{\Delta Q}{\Delta C}u = \left(\frac{0.0032}{0.002212}\right)0.05 = 0.072 \tag{111}$$

Furthermore, the binary (bulk) diffusion coefficient of oxygen and nitrogen is assumed to be constant in this study. However, one better, more accurate way to define it can be written as follows [18]:

$$D_{bulk} = \frac{a}{P}\left(\frac{T}{\sqrt{T_{cr,O_2}T_{cr,N_2}}}\right)^b (P_{cr,O_2}P_{cr,N_2})^{1/3}(T_{cr,O_2}T_{cr,N_2})^{5/12} \times \sqrt{\left(\frac{1}{M_{O_2}}+\frac{1}{M_{N_2}}\right)} \tag{112}$$

where, $a = 2.745\text{E}{-4}$, and $b = 1.823$. The critical temperatures of oxygen and nitrogen are 154 K and 126 K, and the critical pressures are 5050 kPa (49.84 atm) and 3390 kPa (33.46 atm), respectively (Ref. [2, p. 486]). The molecular weights are 32 kg/kmol and 28 kg/kmol for oxygen and nitrogen, respectively. Using these constants, Eq. (112) can be rewritten as in Eq. (113).

$$D_{bulk} = 2.0124E - 4T^bP^{-1} \tag{113}$$

Since, the diffusion ratio is inversely proportional to D_{bulk}, then the following equations can be estimated for the differential of diffusion ratio with respect to temperature and pressure under a simple assumption of $D_{eff} \neq f(T,P)$.

$$\frac{\partial Q}{\partial T} = -b4963T^{-b-1}P = -9.83E - 4 \tag{114}$$

$$\frac{\partial Q}{\partial P} = 4963T^{-b} = 0.1578 \tag{115}$$

Assuming the differential uncertainty of temperature and pressure are 0.1 K and 0.1 atm, the related uncertainties become:

$$\frac{\partial Q}{\partial T}u_T = -9.83E - 4 \cdot 0.1 = -9.83E - 5 \tag{116}$$

$$\frac{\partial Q}{\partial P}u_P = 0.1578 \cdot 0.1 = 0.01578 \tag{117}$$

Hence, the total uncertainty of the current experimental set up is calculated as follows.

$$u_Q = \sqrt{\sum_{i=1}^{n}\left(\frac{\partial Q}{\partial x_i}u_i\right)^2} = \sqrt{(-9.83E-5)^2 + 0.01578^2 + 0.072^2} = 0.0737 \tag{118}$$

References

[1] W.A. Wakeham, A. Nagashima, J.V. Sengers, Measurement of the Transport Properties of Fluids, Blackwell Scientific Publications, 1991. p. 294.
[2] M.M. Mench, Fuel Cell Engines, John Wiley & Sons, 2008.
[3] S. Göll, M. Piesche, Multi-component gas transport in micro-porous domains: multidimensional simulation at the macroscale, Int. J. Heat Mass Transfer 55 (2012) 480–487.
[4] J. Shen, J. Zhou, N.G.C. Astrath, T. Navessin, Z.S. (Simon) Liu, C. Lei, J.H. Rohling, D. Bessarabov, S. Knights, S. Ye, Measurement of effective gas diffusion coefficients of catalyst layers of PEM fuel cells with a Loschmidt diffusion cell, J. Power Sources 196 (2011) 674–678.
[5] N.G.C. Astrath, J. Shen, F.B.G. Astrath, J. Zhou, C. Huang, X.Z. Yuan, H. Wang, T. Navessin, Z.S. Liu, G. Vlajnic, D. Bessarabov, X. Zhao, Note: determination of effective gas diffusion coefficients of stainless steel films with differently shaped holes using a Loschmidt diffusion cell, Rev. Sci. Instrum. 81 (2010) 046104.
[6] N. Zamel, N.G.C. Astrath, X. Li, J. Shen, J. Zhou, F.B.G. Astrath, H. Wang, Z.S. Liu, Experimental measurements of effective diffusion coefficient of oxygen–nitrogen mixture in PEM fuel cell diffusion media, Chem. Eng. Sci. 65 (2010) 931–937.
[7] C. Chan, N. Zamel, X. Li, J. Shen, Experimental measurement of effective diffusion coefficient of gas diffusion layer/microporous layer in PEM fuel cells, Electrochim. Acta 65 (2012) 13–21.
[8] N. Zamel, X. Li, J. Shen, Correlation for the effective gas diffusion coefficient in carbon paper diffusion media, Energy Fuels 23 (2009) 6070–6078.
[9] J.H. Rohling, J. Shen, C. Wang, J. Zhou, C.E. Gu, Photothermal deflection measurement of effective gas diffusion coefficient of a porous medium, Eur. Phys. J. Spec. Top. 153 (2008) 111–113.
[10] J. Crank, The Mathematics of Diffusion Bristol, second ed., Oxford University Press, England, 1975.
[11] H. Carslaw, J.C. Jaeger, Conduction of Heat in Solids, second ed., Oxford, London, 1959.
[12] R. Haberman, Elementary Applied Partial Differential Equations 2e, Prentice Hall, 1987. p. 249.
[13] R. Courant, K.O. Friedrichs, H. Lewy, Ueber die partiellen Differenzgleichungen der mathematische Physik, Math. Ann. 100 (1928) 32–74.
[14] G.P. Peters, D.W. Smith, Numerical study of boundary conditions for solute transport through a porous medium, Int. J. Numer. Anal. Methods Geomech. 25 (2001) 629–650.
[15] F.J. Leij, J.H. Dane, M.T. Vangenuchten, Mathematical analysis of one-dimensional solute transport in a layered soil profile, Soil Sci. Soc. Am. J. 55 (1991) 944–953.
[16] V. Alexiades, Overcoming the stability restriction of explicit schemes via super-time-stepping, in: 2nd International Conference on Dynamic Systems and Applications, Atlanta, May 1995.
[17] V. Alexiades, G. Amiez, P.A. Gremaud, Super-time-stepping acceleration of explicit schemes for parabolic problems, Commun. Numer. Methods Eng. 12 (1996) 31–42.
[18] R.B. Bird, W.E. Stewart, E.N. Lightfoot, Transport Phenomena 2e, John Wiley and Sons, 2007. p. 521.